Journal of Computational Physics 290 (2015) 336–351

Contents lists available at ScienceDirect

Journal of Computational Physics

www.elsevier.com/locate/jcp

A mass-conserved diffuse interface method and its application for incompressible multiphase flows with large density ratio

Y. Wang [a], C. Shu [a,*], J.Y. Shao [a], J. Wu [b], X.D. Niu [c]

[a] Department of Mechanical Engineering, National University of Singapore, 10 Kent Ridge Crescent, Singapore 119260, Singapore
[b] Department of Aerodynamics, College of Aerospace Engineering, Nanjing University of Aeronautics and Astronautics, Nanjing 210016, China
[c] College of Engineering, Shantou University, 243 Daxue Road, Shantou 515063, China

ARTICLE INFO

Article history:
Received 5 December 2014
Accepted 5 March 2015
Available online 10 March 2015

Keywords:
Diffuse interface method
Mass conservation
Lattice Boltzmann flux solver
Multiphase flow
Large density ratio

ABSTRACT

In this work a mass-conserved diffuse interface method is proposed for simulating incompressible flows of binary fluids with large density ratio. In the method, a mass correction term is introduced into the Cahn–Hilliard equation to compensate the mass losses or offset the mass increases caused by the numerical and modeling diffusion. Since the mass losses or increases are through the phase interfaces and at each time step, their values are very small, to keep mass conservation, mass sources or sinks are introduced and uniformly distributed in the volume of diffuse layer. With the uniform distribution, the mass correction term representing mass sources or sinks is derived analytically by applying mass conservation principle. By including the mass correction, the modified Cahn–Hilliard equation is solved by the fifth-order upwind scheme to capture the phase field of the bindery fluids. The flow field is simulated by the newly-developed multiphase lattice Boltzmann flux solver [20]. The proposed approach is validated by simulating the Laplace law, the merging of two bubbles, Rayleigh–Taylor instability and bubble rising under gravity with density ratio of 1000 and viscosity ratio of 100. Numerical results of interface shapes and flow properties agree well with both analytical solutions and benchmark data in the literature. Numerical results also show that the mass is well-conserved in all cases considered. In addition, it is demonstrated that the mass correction term at each time step is in the order of $10^{-4}\sim10^{-5}$, which is a small number compared with the magnitude of order parameter.

1. Introduction

In recent years, the diffuse interface (DI) methods [1–6] have attained remarkable popularities in handling the complex multiphase flow problems. They have been successfully applied to one and multiple bubbles rising under gravity [7,8], Rayleigh–Taylor instability of binary fluids [6,9], micron-scale droplet interactions [10,11] and thermo-capillary flows [12,13]. The wide applications of the DI methods are mainly due to their solid theoretical foundation in the phase field theory [1] and powerful capability of handling the complex morphological changes of phase interfaces without knowing their locations.

In general, most of the existing DI methods can be roughly classified into two categories, i.e., the continuum method based on macroscopic conservation laws [4–6] and the kinetic method based on the mesoscopic lattice Boltzmann equations

* Corresponding author.
E-mail address: mpeshuc@nus.edu.sg (C. Shu).

http://dx.doi.org/10.1016/j.jcp.2015.03.005
0021-9991/

(LBEs) [14–16]. The continuum approach directly solves the Navier–Stokes (N–S) equations for flow field and the convective Cahn–Hilliard (C–H) equation for phase field. Initially, efforts were made on the development of reliable approaches for simulating density-matched binary fluid flows. Numerical methods in this category include those of Gurtin et al. [2] and Yue et al. [5]. Later, this method was extended by Boyer [3] and Ding et al. [6] for simulating multiphase flows with large density ratios. The continuum DI approach can easily apply high-order upwind schemes to get more accurate and stable solutions, which are especially useful for the stable discretization of convective terms in the N–S and C–H equations. As compared with the continuum DI approach, the LBE method [9,15,17–21] has been developed into an alternative powerful tool. Many effective LB models have been successfully developed, such as the thermodynamically consistent model of Swift et al. [16], double-distribution-function (DDF) model of He et al. [9], projection-like LB model of Inamuro et al. [17], the improved DDF model with stable discretization of Lee and his co-workers [18,22]. These marvelous multiphase LB models share the same distinguished features of the LBM, such as high efficiency, simple implementation and intrinsic kinetic nature. Both the continuum and kinetic DI methods have achieved remarkable success in simulating various interfacial flows [23].

In the applications of the DI methods, a critical issue is to guarantee mass conservation for each phase. However, due to appearance of the diffusion term and numerical dissipation introduced in discretization of the convective term in the C–H equation, the total mass of either phase of the binary fluids cannot be conserved exactly. This phenomenon has been witnessed by many researchers [8,24,25]. For example, van der Sman and van der Graaf [25] showed that the mass of a droplet under shear decreases continuously in the long-time evolution. Huang et al. [26] showed that the volume of a rising bubble with incompressible conditions can be decreased by 75% in an extreme case. In addition, Zheng at al. [24] also showed that the DI method may produce a spontaneous, non-physical shrinkage of a bubble, whose volume may continuously be reduced to zero. This mass non-conservation issue of the DI method gets even worse for multiphase flows with large density ratio since for this case, large numerical dissipation is needed to get a stable solution.

To date, the mass non-conservation issue of the DI methods has not been fully resolved. In fact, there are very few works on this topic to the best of our knowledge. Usually, fine grids and small thickness of interfaces are used in the DI methods to improve mass conservation in the numerical solutions [27,28]. This is because fine grids and small thickness of interface can reduce numerical dissipation and mass loss/increase through the interface. Aland and Voigt [27] applied adaptive grids and small values of the interface thickness to solve the C–H equation and obtained grid-independence solutions for the bubble rising problem. Ding and Yuan [28] adopted a dual-resolution Cartesian grid to solve the N–S and C–H equations, in which the flow field is solved on a coarse grid while the phase field is obtained on the finer grid. Although the finer grid may give more accurate results, the computational time is also increased. More importantly, the mass non-conservation problem of the DI method is not completely resolved. Recently, Son [29] introduced an artificial correction equation for the order parameter to keep the mass conservation, which needs additional efforts for the order parameter in each time step. By using this method, Chao et al. [30] presented a filter-based, mass-conserved LBE approach and successfully get accurate results with mass conservation in low Eotvos number. Huang et al. [8] showed that, for the bubble rising problem, the mass is only roughly conserved at high Eotvos and Reynolds numbers, which may experience large oscillations with amplitude of about 10% [8]. In addition, the physical meaning of the artificial correction equation for the order parameter is still unclear.

In this paper, we aim to develop a mass-conserved DI method for effective simulation of multiphase flows with large density ratio. Our development is based on mass conservation principle. As shown in [6], the C–H equation can be derived from the mass conservation law. However, when C–H equation is solved to capture the interface, it involves physical diffusion by the diffusion term and numerical diffusion from discretization of convective term. In fact, the mass loss or increase in a phase state is through the interface by diffusion. If at each time step, we can compensate the mass loss or offset the mass increase in the volume of diffuse layer, we can well keep the mass conservation. Physically, this can be done by distributing mass sources (for the case of mass loss) or sinks (for the case of mass increase) in the diffuse layer. As mass loss or increase is very small at each time step, we can assume that the distribution of mass sources or sinks is uniform. Mathematically, as C–H equation reflects the mass conservation, we can simply add a mass correction term (mass sources or sinks) in the C–H equation. The correction term in the C–H equation only takes a value in the diffuse layer. In other regions, it takes zero. In this work, the modified C–H equation is solved by the fifth-order upwind scheme. In the meantime, the recently-developed multiphase lattice Boltzmann flux solver (MLBFS) [20], which effectively removes the drawbacks of the conventional LBM [31,32] and is capable of simulating multiphase flows with large density ratio, is applied to give the flow field. The reliability of the proposed DI method will be validated by simulating the Laplace law, the merging of two bubbles, Rayleigh–Taylor instability and rising bubble with density ratio of 1000.

2. Methodology

2.1. Mass-conserved DI method for interface capturing

2.1.1. Original Cahn–Hilliard equation

In the DI methods, the Cahn–Hilliard model is usually applied to capture the interfacial evolution of incompressible multiphase flows. The governing equation of this model can be written as:

$$\frac{\partial C}{\partial t} + \nabla \cdot (\boldsymbol{u} C) = \Gamma \nabla^2 \mu_C, \tag{1}$$

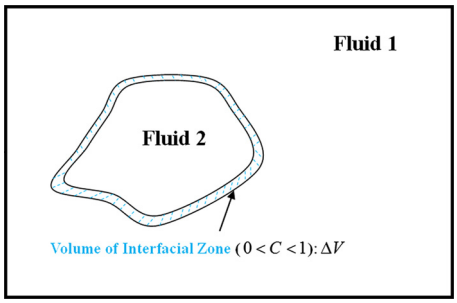

Fig. 1. Illustration of flow domain for binary fluid flows.

where C is the volume fraction of heavier fluids in the range of $[0, 1]$; Γ is known as the mobility or diffuse flow rate. C is also named the order parameter. In Eq. (1), μ_C represents the chemical potential given by the total free energy of fluid–fluid or fluid–wall interfaces, which can be written as:

$$\mu_C = 2\beta C(C-1)(2C-1) - \kappa\nabla^2 C. \tag{2}$$

Here β and κ are constants determined by the interface thickness ξ and the surface tension coefficient σ:

$$\sigma = \sqrt{2\kappa\beta}/6; \quad \kappa = \beta\xi^2/8. \tag{3}$$

With the aid of the Cahn–Hilliard model, the local density ρ is taken as a linear combination of the heavier and lighter fluids (ρ_H and ρ_L):

$$\rho = \rho_L + C\Delta\rho; \quad \Delta\rho = \rho_H - \rho_L \tag{4}$$

2.1.2. Modified Cahn–Hilliard equation with mass correction

Due to the presence of diffusion term and numerical dissipation in discretization of convective term, the total mass of heavier fluid or lighter fluid obtained by solving Eq. (1) cannot be kept conservation in general. Mass loss or increase is usually through the interface between fluids. To resolve this problem, a source term q is introduced into the C–H equation to compensate mass loss or offset the mass increase. The modified C–H equation can be written as:

$$\frac{\partial C}{\partial t} + \nabla\cdot(\boldsymbol{u}C) = \Gamma\nabla^2\mu_C + q \tag{5}$$

It should be noted that the source term q only takes effect in the interfacial zone (layer) and is zero in other regions since the mass loss or increase only takes place in the interfacial zone. q is actually the mass source or sink. To get the expression of q, it is assumed that q is uniformly distributed in the interfacial zone. This assumption is rational since the mass correction at each time step is very small. With this assumption, the correction term q is independent of physical locations and is only a function of time. Integrating Eq. (5) in the volume Ω_L occupied by the phase with lighter fluid as shown in Fig. 1, the resultant equation can be written as:

$$\int_{\Omega_L}\frac{\partial C}{\partial t}dV + \int_S \boldsymbol{u}C d\boldsymbol{S} = \int_{\Omega_L}\Gamma\nabla^2\mu_C dV + \int_{\Omega_L} q dV \tag{6}$$

where S is the boundary of the volume Ω_L. As the mass conservation law is satisfied at the end of each time step, the term $\int_S \boldsymbol{u}C d\boldsymbol{S}$, which represents the total mass flow rate coming into the lighter phase, should be zero, i.e.:

$$\int_S \boldsymbol{u}C d\boldsymbol{S} = 0 \tag{7a}$$

In addition, from Eq. (4), we have the following relationship:

$$\int_{\Omega_L}\frac{\partial C}{\partial t}dV = \frac{1}{\Delta\rho}\cdot\frac{\partial}{\partial t}\int_{\Omega_L}\rho dV = \frac{1}{\Delta\rho}\cdot\frac{\partial M_L}{\partial t} \tag{7b}$$

where M_L is the mass of the lighter fluid.

With assumption of uniform distribution of q, we have

$$\int_{\Omega_L} q dV = q\Delta V \tag{7c}$$

where ΔV is the volume of the interfacial zone shown in Fig. 1. Note that $q = 0$ outside this zone. Substituting Eq. (7) into Eq. (6), the expression of the mass correction term q in the interfacial zone $(0 < C < 1)$ can be derived. Overall, the final expression of q can be written as

$$q = \begin{cases} \dfrac{1}{\Delta V} \cdot \left(\dfrac{1}{\Delta \rho} \dfrac{\partial M_L}{\partial t} - \displaystyle\int_{\Omega_L} \Gamma \nabla^2 \mu_C dV \right), & 0 < C < 1 \\ 0, & \text{elsewhere} \end{cases} \tag{8}$$

Note that the term $\Gamma \nabla^2 \mu_C = 0$ is applied in the flow field far from the interfacial zone. From the above derivation, it can be seen that the mass correction term q has a clear physical meaning. Due to numerical dissipation, the total mass of either phase of binary fluids obtained from the numerical solutions is not conserved. The mass loss in a unit time can be quantified by the mass correction term q and is added back into the interfacial zone. As a result, the total mass can be conserved. In the numerical validation, we will verify the effectiveness of the proposed method and we will further show that the correction term q is in the order of $10^{-5} \sim 10^{-4}$ in all cases considered, which is very small as compared with the magnitude of the order parameter, $C \sim O(1)$. This is consistent with assumption of uniform distribution for the mass correction in the interfacial zone.

2.1.3. Numerical discretization

To numerically solve Eq. (5), the fifth-order Weighted Essentially Non-oscillatory scheme (WENO) [33] is applied to discretize the convection term $\nabla \cdot (\boldsymbol{u}C)$ and the second-order difference scheme is applied to discretize $\Gamma \nabla^2 \mu_C$. As the discretization procedure is standard, the detail will not be shown in the paper.

In addition to $\nabla \cdot (\boldsymbol{u}C)$ and $\Gamma \nabla^2 \mu_C$, the mass correction term q in the interfacial zone should also be computed numerically. In the present study, this term is approximated by:

$$q = \frac{1}{\Delta V} \cdot \left(\frac{1}{\Delta \rho} \frac{\partial M_L}{\partial t} - \int_{\Omega_L} \Gamma \nabla^2 \mu_C dV \right) = \frac{1}{\Delta V} \cdot \left(\frac{\Delta M}{\Delta \rho \cdot \Delta t} - \sum_{\Omega_L} \Gamma \nabla^2 \mu_C \cdot dV \right) \tag{9}$$

where $\Delta M = M^n - M^0$, Δt is the time step and $\Gamma \nabla^2 \mu_C$ is numerically calculated. In practical applications, the correction term q is applied in the zone of $0.1 \le C \le 0.9$ to avoid possible numerical errors in the identification of the interfacial zone. Here, M^0 is the total mass of the lighter phase at $t = t_0$ and M^n is the total mass of the same phase at $t = t_n$. The mass at any time can be computed by the following equation [34]:

$$M^n = \int_{C \le 0.5} \rho dV = \rho_L V_L^n \tag{10}$$

With Eqs. (9) and (10), the total volume can also be conserved, which is consistent with the incompressible condition for incompressible multiphase flows.

2.2. Multiphase lattice Boltzmann flux solver for the flow field

2.2.1. Governing equations

To effectively solve the flow field of the incompressible binary fluids, the recently-developed multiphase lattice Boltzmann flux solver (MLBFS) [20] is applied. The MLBFS directly solves the incompressible N–S equations while the fluxes at each cell interface are reconstructed locally by application of standard LBE solutions. The governing equations, which are recovered by the multiphase LBE model [18,22], can be written as:

$$\left(\frac{\partial p}{\partial t} + \boldsymbol{u} \cdot \nabla p \right) + \rho c_s^2 \nabla \cdot \boldsymbol{u} = 0, \tag{11a}$$

$$\frac{\partial \rho \boldsymbol{u}}{\partial t} + \nabla \cdot (\rho \boldsymbol{u} \otimes \boldsymbol{u}) = -\nabla p + \nabla \left[\mu \cdot \left(\nabla \boldsymbol{u} + (\nabla \boldsymbol{u})^T \right) \right] + \boldsymbol{F}_s, \tag{11b}$$

where $\boldsymbol{F}_s$ is the surface tension. By applying the relationships between the macroscopic fluxes and the density distribution functions, Eq. (11) can be rewritten as [20]:

$$\frac{\partial p}{\partial t} + \nabla \cdot \left(\sum_{\alpha=0}^{N} \boldsymbol{e}_\alpha f_\alpha^{eq} \right) + \boldsymbol{u} \cdot \nabla \left(p - \rho c_s^2 \right) = 0, \tag{12a}$$

$$\frac{\partial \rho \boldsymbol{u} c_s^2}{\partial t} + \nabla \cdot \left(\Pi - \mu \Pi^e \right) - \boldsymbol{F}_s c_s^2 = 0, \tag{12b}$$

where

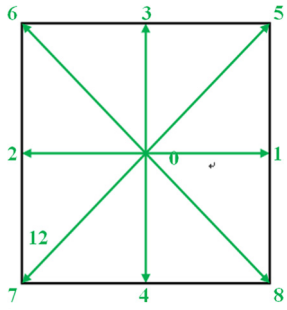

Fig. 2. The D2Q9 lattice velocity model.

$$\Pi_{\beta\gamma} = \sum_{\alpha=0}^{N} (\boldsymbol{e}_\alpha)_\beta (\boldsymbol{e}_\alpha)_\gamma \hat{f_\alpha} \tag{12c}$$

$$\hat{f_\alpha} = f_\alpha^{eq} + \left(1 - \frac{1}{2\tau}\right) f_\alpha^{neq} \tag{12d}$$

$$f_\alpha^{neq} = -\tau \delta_t \left(\frac{\partial}{\partial t} + \boldsymbol{e}_\alpha \cdot \nabla\right) f_\alpha^{eq} \tag{12e}$$

$$\Pi_{jk}^{e} = \frac{1}{\rho}\left(u_j \frac{\partial}{\partial x_k} + u_k \frac{\partial}{\partial x_j}\right)\left(p - \rho c_s^2\right) \tag{12f}$$

In Eq. (12), $\boldsymbol{e}_\alpha$ is the particle velocity in the α direction, and f_α^{eq} is the equilibrium density distribution function:

$$f_\alpha^{eq}(\boldsymbol{r}, t) = w_\alpha \left[p + \rho c_s^2 \left(\frac{\boldsymbol{e}_\alpha \cdot \boldsymbol{u}}{c_s^2} + \frac{(\boldsymbol{e}_\alpha \cdot \boldsymbol{u})^2 - (c_s|\boldsymbol{u}|)^2}{2c_s^4}\right)\right], \tag{13}$$

where the coefficients w_α and the sound speed c_s depend on the lattice velocity model. If the popular D2Q9 model is applied as shown in Fig. 2, the coefficients w_α and the sound speed c_s are given as $w_0 = 4/9$, $w_1 = w_2 = w_3 = w_4 = 1/9$ and $w_5 = w_6 = w_7 = w_8 = 1/36$, $c_s = c/\sqrt{3}$.

The surface tension force $\boldsymbol{F}_s$ has many different forms. In the present study, the continuous form of Kim [35], which is proven to have a better performance and is free from the wiggle effects [30], is applied:

$$\boldsymbol{F}_s = -\kappa \nabla \cdot \left(\frac{\nabla C}{|\nabla C|}\right) |\nabla C| \nabla C \tag{14}$$

2.2.2. Finite volume discretization

In the MLBFS, a cell-centered finite volume method is applied to discretize Eq. (12) spatially and the third order TVD (Total Variation Diminishing) Runge–Kutta scheme is applied to march in time for the flow variables ($\boldsymbol{W} = (p, \rho u c_s^2, \rho v c_s^2)$) at each cell center. Integrating Eq. (12) over a control volume Ω_i gives [20]:

$$\frac{d\boldsymbol{W}_i}{dt} = -\frac{1}{\Delta V_i} \sum_k \boldsymbol{R}_k \Delta S_k + \boldsymbol{F}_E, \tag{15}$$

$$\boldsymbol{F}_E = \left(-\boldsymbol{u} \cdot \nabla\left(p - \rho c_s^2\right), c_s^2 F_{sx}, c_s^2 F_{sy}\right)^T, \tag{16}$$

where ΔV_i is the volume of Ω_i, and ΔS_k is the area of the kth control surface enclosed Ω_i. With the popular D2Q9 lattice velocity model, the flux $\boldsymbol{R}_k$ at a cell interface can be written as:

$$\boldsymbol{R}_k = \begin{bmatrix} n_x(f_1^{eq} - f_2^{eq} + f_5^{eq} - f_6^{eq} - f_7^{eq} + f_8^{eq}) + n_y(f_3^{eq} - f_4^{eq} + f_5^{eq} + f_6^{eq} - f_7^{eq} - f_8^{eq}) \\ n_x(\hat{f_1} + \hat{f_2} + \hat{f_5} + \hat{f_6} + \hat{f_7} + \hat{f_8} - \mu \cdot \Pi_{11}^e) + n_y(\hat{f_5} - \hat{f_6} + \hat{f_7} - \hat{f_8} - \mu \cdot \Pi_{12}^e) \\ n_x(\hat{f_5} - \hat{f_6} + \hat{f_7} - \hat{f_8} - \mu \cdot \Pi_{21}^e) + n_y(\hat{f_3} + \hat{f_4} + \hat{f_5} + \hat{f_6} + \hat{f_7} + \hat{f_8} - \mu \cdot \Pi_{22}^e) \end{bmatrix}_k \tag{17}$$

where n_x and n_y are the x and y components of the unit outer normal vector on the kth control surface. In Eq. (17) for the flux $\boldsymbol{R}_k$ at the cell interface, the unknowns are $\hat{f_\alpha}$ and Π_{jk}^e. Since Π_{jk}^e only includes the velocity and the first order derivatives of the density and pressure, the evaluation of this term can be easily done by the finite difference scheme. The key issue is the evaluation of $\hat{f_\alpha}$. Details of the evaluation procedure are given below.

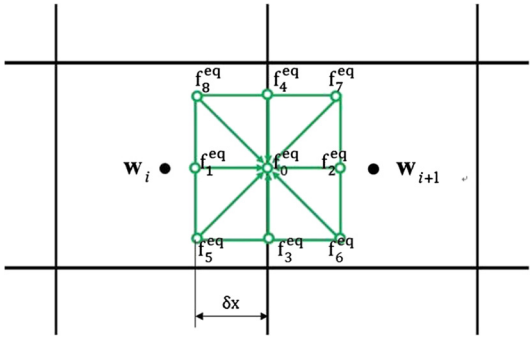

Fig. 3. Flux evaluation at a cell interface, $\boldsymbol{W} = (p, \rho u, \rho v)$.

Evaluation of $\hat{f_\alpha}$ at a cell interface

Consider a cell interface between two adjacent control volumes shown in Fig. 3. The evaluation of $\hat{f_\alpha}$ is performed at the middle point of the interface. $\hat{f_\alpha}$ includes both f_α^{eq} and f_α^{neq} as shown in Eq. (12d).

The non-equilibrium term f_α^{neq} can be approximated by applying the Taylor-series expansion to Eq. (12d), that is,

$$f_\alpha^{neq}(\boldsymbol{r}, t) = -\tau\left[f_\alpha^{eq}(\boldsymbol{r}, t) - f_\alpha^{eq}(\boldsymbol{r} - \boldsymbol{e}_\alpha\delta_t, t - \delta_t)\right] \tag{18}$$

Here, $\boldsymbol{r}$ represents the mid-point of the interface. Following the convention of the LBM, $f_\alpha^{eq}(\boldsymbol{r} - \boldsymbol{e}_\alpha\delta_t, t - \delta_t)$ can be computed from ρ, $\boldsymbol{u}$ and p at $(\boldsymbol{r} - \boldsymbol{e}_\alpha\delta_t, t - \delta_t)$. These flow properties can be obtained easily through interpolation:

$$\psi(\boldsymbol{r} - \boldsymbol{e}_\alpha\delta_t, t - \delta_t) = \begin{cases} \psi(\boldsymbol{r}_i) + (\boldsymbol{r} - \boldsymbol{e}_\alpha\delta_t - \boldsymbol{r}_i)\cdot\nabla\psi(\boldsymbol{r}_i), & \text{when } \boldsymbol{r} - \boldsymbol{e}_\alpha\delta_t \text{ is in } \Omega_i \\ \psi(\boldsymbol{r}_{i+1}) + (\boldsymbol{r} - \boldsymbol{e}_\alpha\delta_t - \boldsymbol{r}_{i+1})\cdot\nabla\psi(\boldsymbol{r}_{i+1}), & \text{when } \boldsymbol{r} - \boldsymbol{e}_\alpha\delta_t \text{ is in } \Omega_{i+1} \end{cases} \tag{19}$$

where $\boldsymbol{r}_i$ and $\boldsymbol{r}_{i+1}$ are the two cell centers of the considered interface and ψ represents $\boldsymbol{u}$ or p. After interpolation, $f_\alpha^{eq}(\boldsymbol{r} - \boldsymbol{e}_\alpha\delta_t, t - \delta_t)$ can be computed using Eq. (13).

$f_\alpha^{eq}(\boldsymbol{r}, t)$ can also be computed by ρ, $\boldsymbol{u}$ and p at $(\boldsymbol{r}, t)$ using Eq. (13). $p(\boldsymbol{r}, t)$ and $\rho(\boldsymbol{r}, t)\boldsymbol{u}(\boldsymbol{r}, t)$ can be constructed by the LBM solution as [31–33]:

$$p(\boldsymbol{r}, t) = \sum_{\alpha=0}^{N} f_\alpha^{eq}(\boldsymbol{r} - \boldsymbol{e}_\alpha\delta_t, t - \delta_t), \tag{20}$$

$$\rho(\boldsymbol{r}, t)\boldsymbol{u}(\boldsymbol{r}, t)c_s^2 = \sum_{\alpha=0}^{N} f_\alpha^{eq}(\boldsymbol{r} - \boldsymbol{e}_\alpha\delta_t, t - \delta_t)\boldsymbol{e}_\alpha, \tag{21}$$

$$\rho(\boldsymbol{r}, t) = \sum_{\alpha=0}^{N} w_\alpha\rho(\boldsymbol{r} - \boldsymbol{e}_\alpha\delta_t, t - \delta_t), \tag{22}$$

where, $f_\alpha^{eq}(\boldsymbol{r} - \boldsymbol{e}_\alpha\delta_t, t - \delta_t)$ has already been evaluated and w_α is the coefficient given previously. By applying Eqs. (13) and (20)–(22), $f_\alpha^{eq}(\boldsymbol{r}, t)$ can be calculated.

Once $f_\alpha^{eq}(\boldsymbol{r} - \boldsymbol{e}_\alpha\delta_t, t - \delta_t)$ and $f_\alpha^{eq}(\boldsymbol{r}, t)$ are calculated, f_α^{neq} can be computed by using Eq. (18) and then $\hat{f_\alpha}$ can be easily obtained by using Eq. (12d).

After obtaining $\hat{f_\alpha}$ and Π_{jk}^e, the flux at any cell interface can be evaluated according to Eq. (17). Then, the flow variables at the cell center can be updated by solving Eq. (15) with the third order TVD temporal scheme.

3. Numerical results and discussion

In this section, the proposed mass-conserved DI method will be validated by simulating the Laplace law for a static bubble, the merging of two bubbles under capillary force, Rayleigh–Taylor instability and bubble rising under gravity with large density ratio and viscosity ratio. Much attention will be paid to its performance in conserving the mass.

3.1. Laplace law

The Laplace law for a static bubble (density ρ_L) immersed in another fluid (density ρ_H) is studied here to examine the performance of the present solver in conserving the mass. This law describes the relationship between the pressure difference across the phase interface and the surface tension force:

$$p_{in} - p_{out} = \frac{\sigma}{R} \tag{23}$$

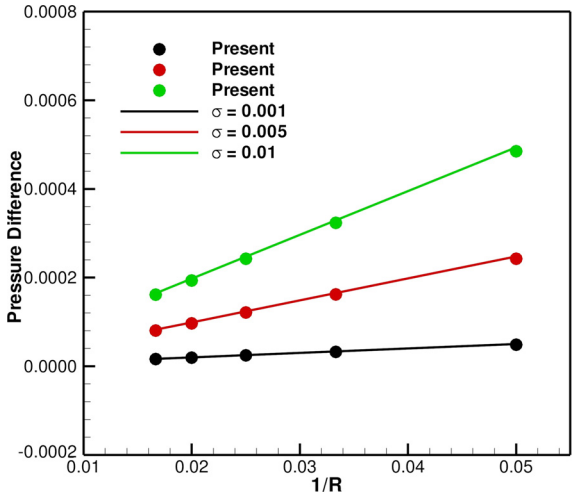

Fig. 4. Pressure difference between the inner and outer of the static bubble with $\sigma = 0.001$, 0.005 and 0.05.

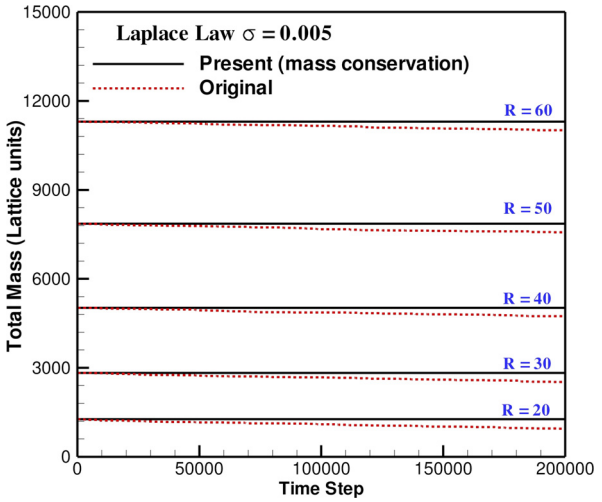

Fig. 5. Evolution of the total mass of the static bubble with different radius at $\sigma = 0.005$.

where p_{in} and p_{out} are the pressure inside and outside the bubble, respectively; σ is the surface tension and R is the radius of the bubble. The profile of the order parameter along the interface can also be given analytically by:

$$C(y) = \frac{1}{2}\left[1 + \tanh(2y/\xi)\right] \tag{24}$$

In the present study, a grid size of 201×201 is applied and natural boundary condition is set at all boundary surfaces. The flow parameters are set as $\rho_H = 10$, $\rho_L = 1.0$, $\nu_H = \nu_L = 0.02$ and $\xi = 5$. The radius of the bubble is varied from 20 to 60.

Fig. 4 shows the pressure difference versus $1/R$ with three different surface tensions of $\sigma = 0.001$, 0.005 and 0.01. As can be seen, the present results agree well with the solutions given by the Laplace law, which verifies the reliability of the proposed solver. Fig. 5 compares the evolution of the total mass of the static bubble in different times for the case of $\sigma = 0.005$. Also included in this figure are the results of the original method without mass correction. It is clearly shown that the present results conserve mass very well while the mass of the bubble obtained by the original DI method [20] decreases continuously. To quantify these results, the total mass of the static bubble at the time of lattice unit, $t = 200\,000$, is compared in Table 1. Without mass correction, the masses of the bubbles with different size are lost from 25.31% to 2.62%. The advantage of the present solver in conserving the mass is obvious. Fig. 6 compares the profile of the order parameter C along the y-centerline of the flow domain for the case of $\sigma = 0.005$ and $R = 50$. The numerical results also agree well with the analytical solution, which implies that the mass correction term q will not spoil the interface shape.

Table 1
Comparison of the total mass for the static bubble at $t = 200\,000$.

Radius	Initial mass	Final mass			
		Original method	Relative error	Present	Relative error
20	1264	944	25.31%	1264	0
30	2828	2520	10.89%	2828	0
40	5024	4720	6.05%	5024	0
50	7860	7572	3.66%	7860	0
60	11 304	11 008	2.62%	11 304	0

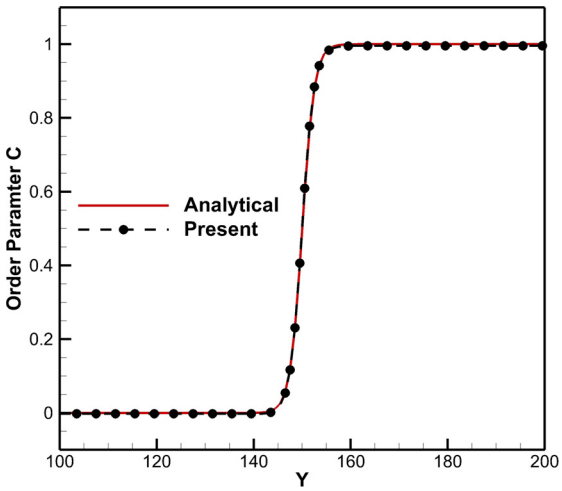

Fig. 6. Comparison of the profile of the order parameter with the analytical solution for $\sigma = 0.005$ and $R = 50$.

3.2. Two merging bubbles

Two merging bubbles, which involve complex topological changes of the interface, are considered in this section to further validate the present solver. Previous studies [19] show that, when the gap d between the two bubbles is less than twice of the interface thickness 2ξ, merging will occur due to surface tension force. To mimic this phenomenon, the computational domain is set as $[0, 240] \times [0, 200]$ in lattice units and natural boundary condition is applied at all boundaries. Initially, the two bubbles with identical radius of $R = 25$ are respectively placed at $(92, 100)$ and $(148, 100)$, which gives a gap of $d = 6$. The flow parameters are set as: $\rho_H = 10$, $\rho_L = 1.0$, $\nu_H = \nu_L = 0.02$, $\sigma = 0.005$ and $\xi = 4$. With these parameters, it can be calculated that $d < 2\xi$, which implies that the merging will take place.

Fig. 7 shows the evolution of the interfacial shapes of two bubbles merging under capillary force at different time. It can be easily observed that the two bubbles gradually merge together and finally form a larger bubble. Fig. 8 compares the final bubble size of the present method with those of analytical prediction and the original DI method [20]. As shown in this figure, the bubble radius obtained by the original method is reduced by 3.81% as compared with the analytical solution while the bubble radius with mass correction agrees excellently well with the theoretical prediction. This comparison verifies the capability of the present method for conserving the mass. Fig. 9 shows the instantaneous mass correction term q in the merging process. The maximum magnitude of q is less than 5×10^{-4} in this case, which is very small as compared with the order parameter C (in the order of $O(1)$). The small value of q is also consistent with the assumption that the mass correction can be uniformly distributed in the interfacial zone.

3.3. Rayleigh–Taylor instability

The Rayleigh–Taylor instability of binary fluids [6,9,20], which involves complex interfacial interactions, is studied in this section. This problem takes place in a rectangular box of $\Omega = [-d/2, d/2] \times [-2d, 2d]$, which is filled with two layers of fluids, heavy fluid (density ρ_H) on top of light one (density ρ_L). The interface of these two fluids is initially perturbed by specifying its position with a cosine function of $y(x) = 0.1d\cos(2\pi x/d)$. Periodic condition is applied to the left and right boundaries and no-slip condition is used to the upper and lower walls. This problem is governed by two non-dimensional parameters: the Reynolds number $\mathrm{Re} = \sqrt{dg} \cdot d/\nu$ and the Atwood number $At = (\rho_H - \rho_L)/(\rho_H + \rho_L)$, where d is the width of the rectangular box and g is the gravitational acceleration. In the present study, the following parameters are applied for simulations: $d = 200$, $\sqrt{dg} = 0.01$, $\rho_L = 1$, $At = 0.5$ and $\mathrm{Re} = 256$.

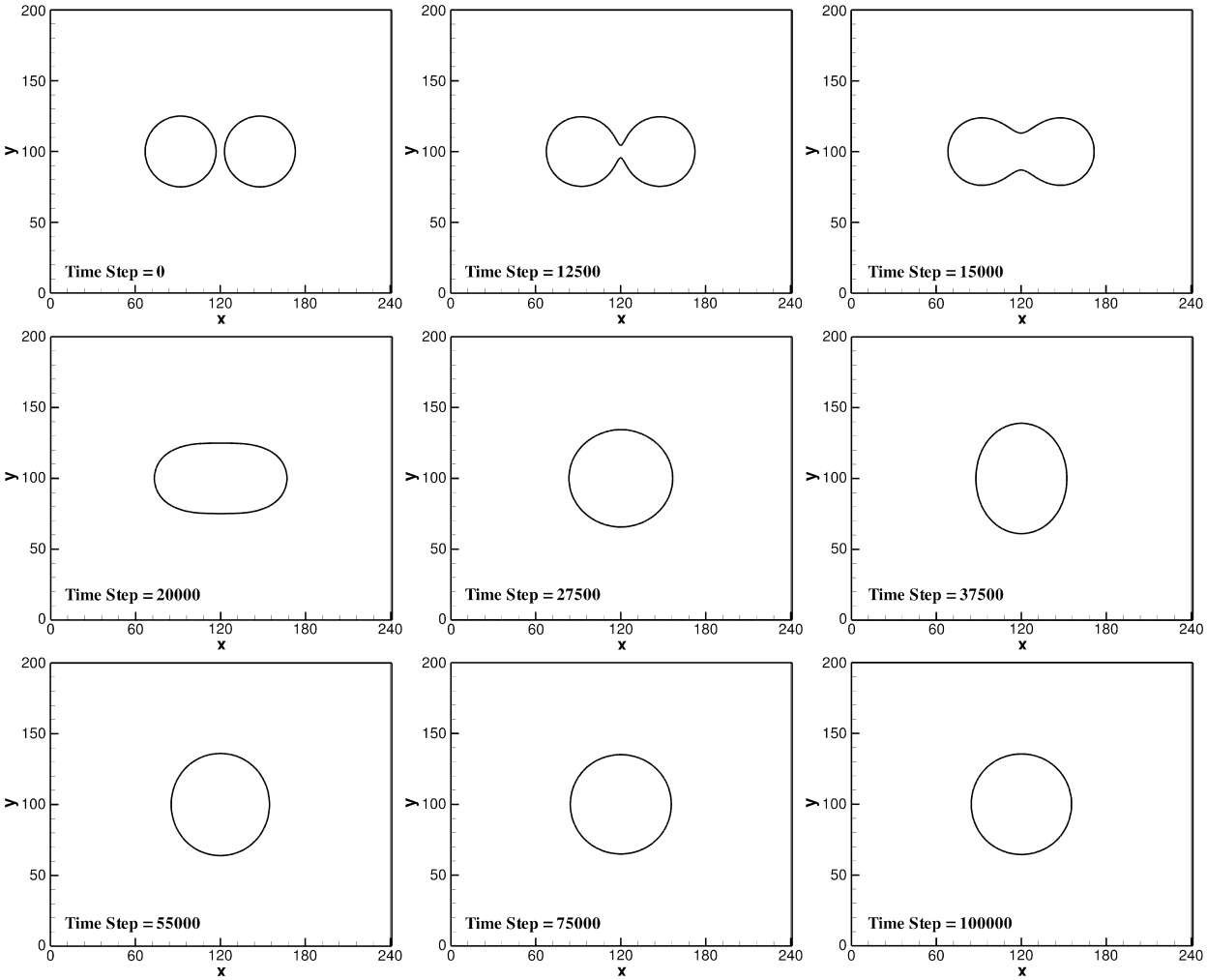

Fig. 7. Evolution of the interfacial shapes for the merging of two bubbles.

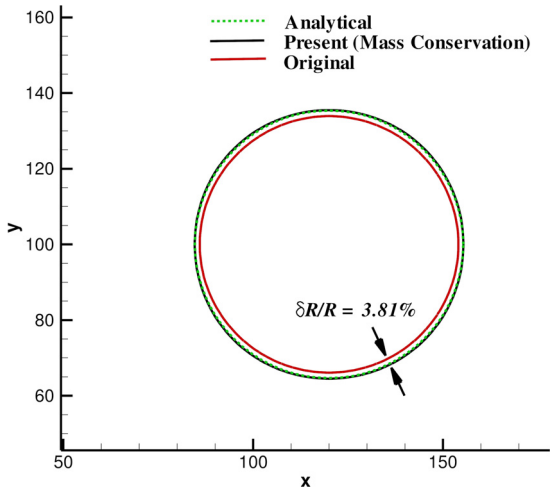

Fig. 8. Comparison of the final shape for the merging of two bubbles.

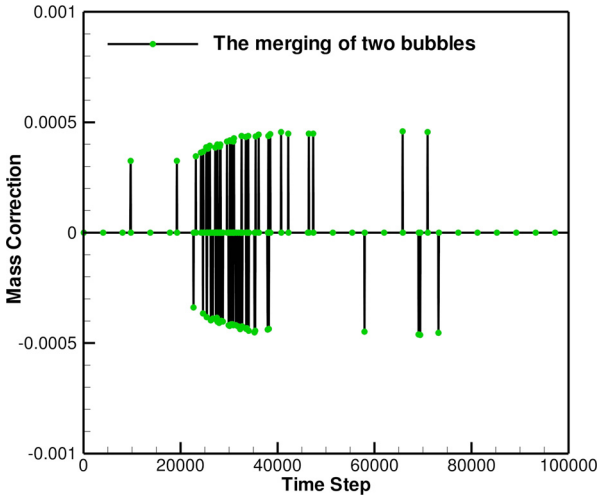

Fig. 9. The evolution of the mass correction term for the merging of two bubbles.

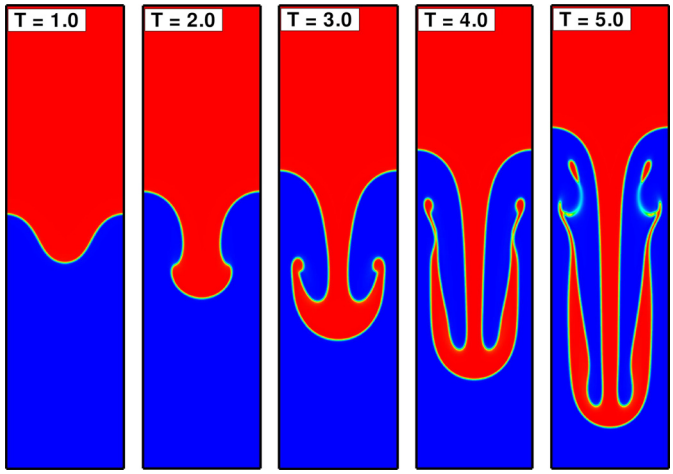

Fig. 10. Evolution of the interface shapes for the Rayleigh–Taylor instability at Re = 256 with mass conservation.

Fig. 10 shows the interfacial morphology at different times. At the initial time of $t = 1$ and 2, the generation of falling spike for heavy fluid and rising bubble for light fluid can be clearly observed. As time continues, the heavy fluid adjacent to the falling spike generates two secondary droplets and gradually sloughs them off due to the well-known Kelvin–Helmholtz instability. These observations agree well with the previous studies [9,20]. To examine whether the mass is conserved in the process, the total mass of the light fluid from $t = 0$ to $t = 5$ is shown in Fig. 11. Also included in this figure are the results of the original DI method [20] for comparison. It is clearly shown that the present results satisfy the mass conservation law perfectly while the results of the original method lose about 1% of the total mass of the light fluid at $t = 5$. Fig. 12 compares the interface positions and velocities of the rising bubble and falling spike with the previous solutions [6,9,20]. Overall, good agreements are achieved. All these agreements verify the reliability of the present solver to study complex interfacial interactions of binary fluid flows with mass conservation.

3.4. Bubble rising with large density ratio

Although the present method has been successfully validated by simulating three binary fluid flow problems, the density ratio and viscosity ratio of these cases are nevertheless small ($\rho_{H/L} \leq 10$). In this section, we will continue to examine the present solver by simulating the rising bubble in water with a density ratio of 1000 and viscosity ratio of 100 [27]. The schematic diagram of this problem is depicted in Fig. 13. A gas bubble of diameter $D = 0.5$ mm is placed at (0.5 mm, 0.5 mm) in a rectangular domain of [0 mm, 1 mm] × [0 mm, 2 mm]. The density and viscosity of the bubble and

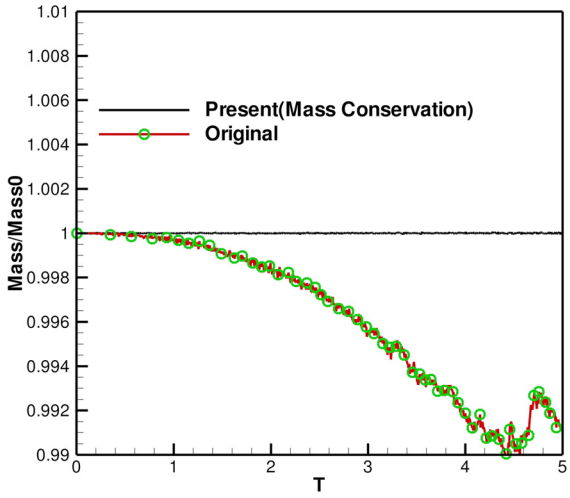

Fig. 11. Evolutions of the total mass of the lighter (bubble) phase.

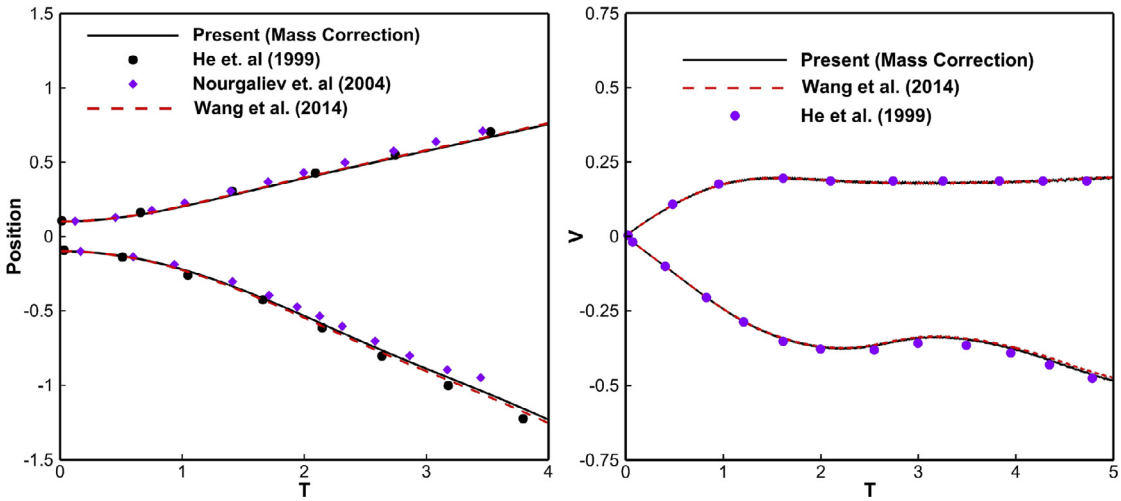

(a) Interface positions (b) interface velocities

Fig. 12. Comparison of the interface positions and velocities for the Rayleigh–Taylor instability at Re = 256.

Table 2
Flow parameters for the bubble rising under gravity.

Cases	Eo	Re	$D_{lattice}$	U	ρ_H	μ_H	ρ_H/ρ_L	μ_H/μ_L
1	125							
2	50	35	120	0.0012	100	0.36	1000	100
3	10							

the surrounding fluid are noted respectively as: ρ_L, μ_L and ρ_H, μ_H. In this problem, the Reynolds number Re and the Eotvos number Eo, can be defined respectively as:

$$\mathrm{Re} = \frac{\rho_L g^{1/2} D^{3/2}}{\mu_L} \quad \text{and} \quad Eo = \frac{\rho g D^2}{\sigma}, \tag{25}$$

where g is the gravitational acceleration.

In the present study, the flow parameters are given in Table 2 in detail. As can be seen, Re = 40 and three Eotvos numbers of $Eo = 10,\ 50$ and 125 are used to show the interface shapes of the rising bubbles in different flow regimes. A grid size of 241×481 is applied to discretize the flow domain. No-slip condition is applied on the upper and lower walls and periodic condition is used on the left and right boundaries.

Figs. 14 and 15 compare the interface positions and center of mass Y_p for the bubble rising under gravity with $\rho_{H/L} = 1000$ at $Eo = 125$. Also included in this figure are the benchmark solutions of Aland and Voigt [27], which are obtained on

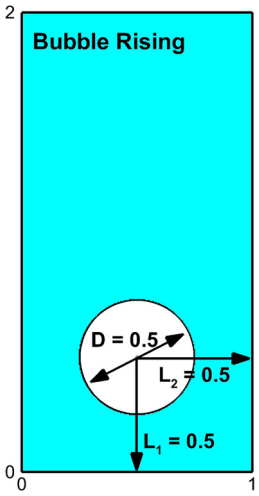

Fig. 13. Illustration of the gas bubble rising in liquid.

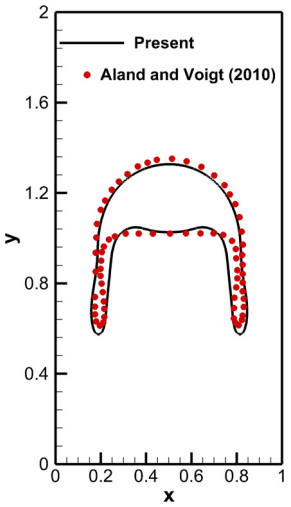

Fig. 14. Comparison of interface positions with the benchmark solutions for the rising bubble with Re = 35 and $Eo = 125$ at $T = 4.2$.

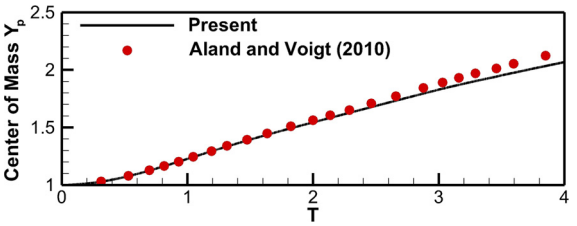

Fig. 15. Comparison of center of mass Y_p with the benchmark solutions for the rising bubble with Re = 35 and $Eo = 125$.

fine adaptive grids with high spatial resolution. It can be seen that the present results for the bubble in a skirted shape and its mass center at $t = 4.2$ agree fairly well with those of published data. For the cases of $Eo = 10$ and 50, the shapes of the bubble at different times are compared with those of the original DI method [20] as shown in Fig. 16. For the rising bubble with $Eo = 10$, at the initial rising time of $T = 1$ s, the interface positions obtained by both methods agree well with each other. As the bubble continues rising to $T = 3$ s, the overall interface shapes and positions are also quite similar in quantity. However, it can be clearly observed that the total volume of the bubble obtained from the original method is slightly smaller than the result of the present approach. When $T = 4$ s, the rising bubble in the present results reaches a steady state and its shape does not change while the volume of the bubble obtained by original approach becomes even smaller. Similar phenomenon can also be observed for the rising bubble in the skirted regime at $Eo = 50$, where large deformations of the

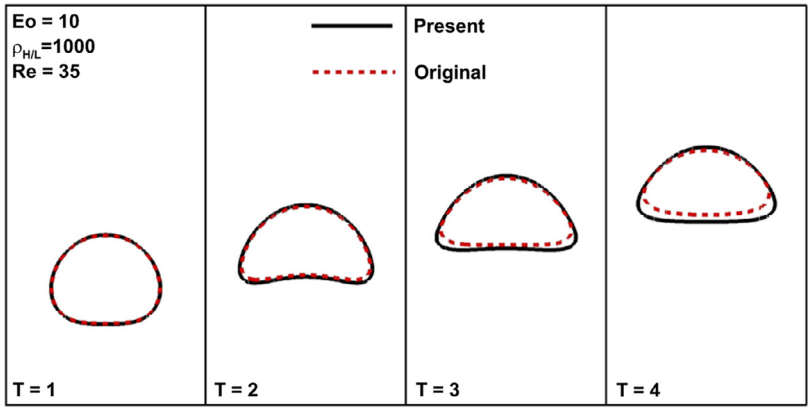

(a) Eo = 50

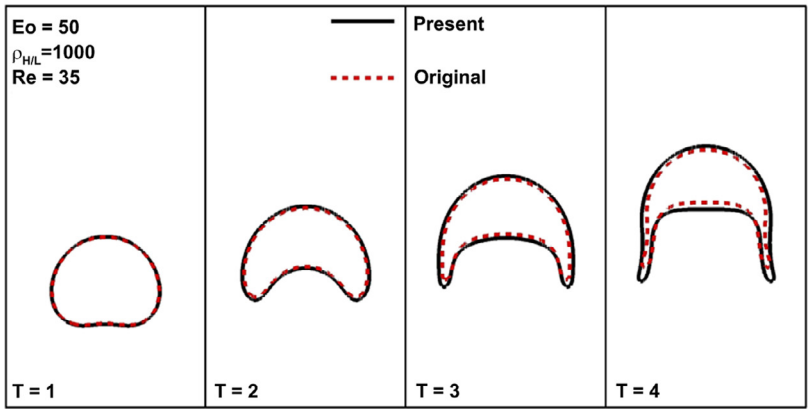

(b) Eo =10

Fig. 16. Comparison of the bubble shape with the original DI method [20] for the rising bubble with Re = 35 and $\rho_{H/L} = 1000$.

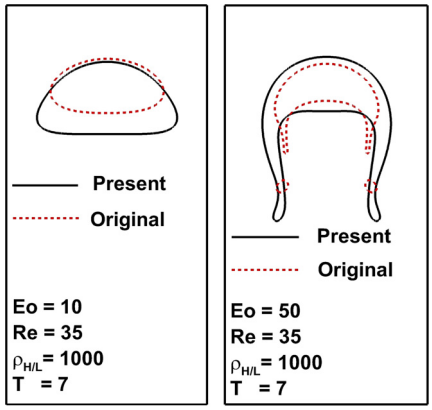

Fig. 17. Comparison of the interface shapes for the rising bubble at $T = 7$.

rising bubble takes place. After a long time evolution, the bubble shapes at $T = 7$ s are compared in Fig. 17. It can be clearly seen from the results of the original method that, the total mass of the rising bubble is reduced substantially and the break of the tails of the bubbles at $Eo = 50$ occurs at $T = 7$ s, which is unphysical for this case. Overall, it can be summarized that, although their shapes are very similar in morphology, the bubbles obtained by the original approach shrink their volume, which is similar to the results of Zheng et al. [24]. This phenomenon means that the conventional DI method fails to guarantee mass conservation. However, from the evolution of the total mass shown in Fig. 18, it is obvious that the mass can be well-conserved by the present approach for all the three cases considered in Figs. 14–17. It can also be seen from Fig. 19 that the mass correction term q is less than 5×10^{-5}, which is much smaller than the typical magnitude of the

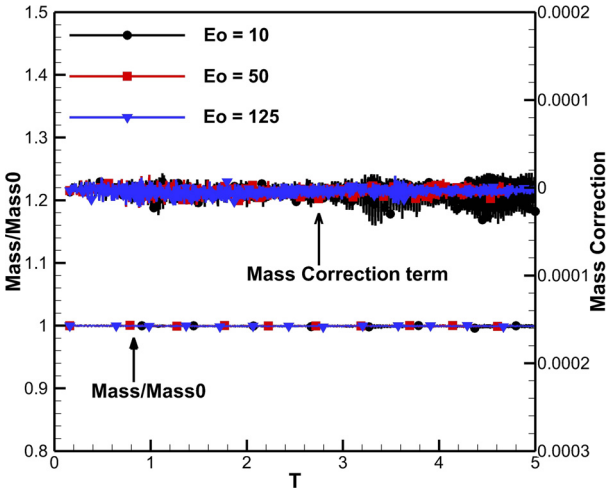

Fig. 18. Evolution of the total mass of the bubble and the mass correction term at Re = 35 with different Eotvos numbers.

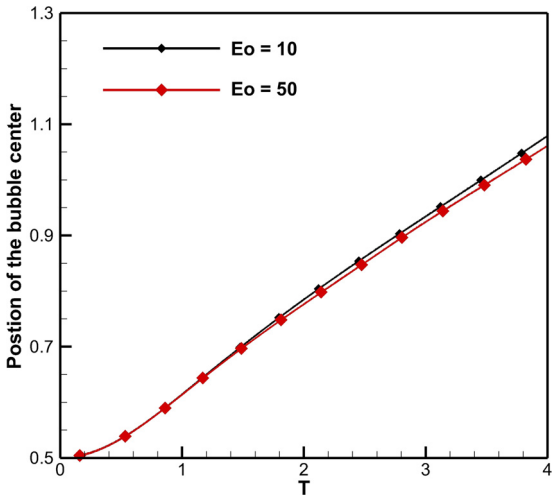

Fig. 19. Evolution of center of mass Y_p for the rising bubble with Re = 35 and $\rho_{H/L} = 1000$.

order parameter ($O(1)$). All these results verify the reliability of the present approach for simulating multiphase flows with mass conservation.

To further demonstrate its performance, the mass center of the bubble at $Eo = 10$ and 50 defined by Aland and Voigt [27] are depicted in Fig. 19, which quantitatively shows the continuously moving-up of the bubble. The flow fields around the bubble at $T = 4$ s obtained by the method with and without mass correction are depicted in Fig. 20. For the case of $Eo = 10$, a pair of vortices are generated behind the bubble, which is similar to the case of flows past a circular cylinder [32]. It can be observed that the vortex from the original DI method is obviously smaller than the present one. This may be due to the fact that the shrinkage of bubble continuously reduces characteristic length and the Reynolds number. At $Eo = 150$, two pairs of vortices are generated at the tail of the bubble, which is also observed in [8]. It can also be seen that both the sizes of the bubble and vortex behind the bubble are obviously reduced in the results obtained by the original DI method due to non-conservation of mass, which further demonstrates the superiority of the present approach over the conventional DI method in keeping the mass conservation.

4. Conclusions

Due to physical and numerical diffusion in solving the C–H equation, the conventional diffuse interface method is not able to conserve the mass accurately. The problem gets even worse for multiphase flows with large density contrast, where the mass may be lost significantly and unphysical results may be produced. To resolve this problem, a mass-conserved diffuse interface method has been proposed in this work by distributing mass sources or sinks in the diffuse layer. In particular, a mass correction term, which takes zero outside the diffuse layer, is introduced into the C–H equation. As mass loss or increase is very small at each time step, it is assumed that the distribution of the mass correction term is uniform

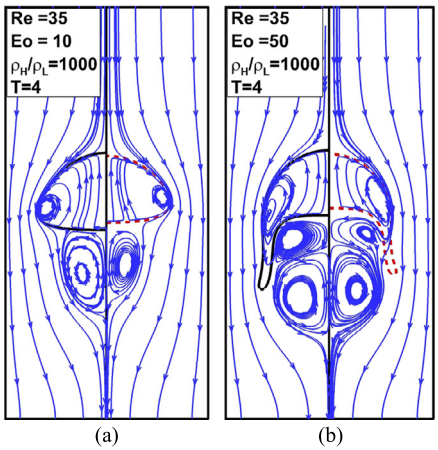

Fig. 20. Streamlines for the rising bubble at $\mathrm{Re} = 35$ and $\rho_{H/L} = 1000$ with different Eotvos numbers (Left panel: the present method with mass conservation; Right panel: the original DI method [20]).

in space and varies with time. The expression of this term is derived analytically by integrating the C–H equation over the sub-domain occupied by the lighter phase of the binary fluids. Together with this correction term, the modified C–H for the phase field is discretized by the fifth-order WENO scheme and the N–S equations for the flow field are solved by the MLBFS. In addition, the surface tension force between interfaces is implemented by using a continuous form, which has been proven to have better performance. As compared with the conventional DI method, which may give unphysical solutions with mass losses, the present method is able to conserve the mass accurately.

The proposed method has been successfully validated through numerical tests of Laplace law, the merging of two bubbles, Rayleigh–Taylor instability and bubble rising under gravity with density ratio of 1000 and viscosity ratio of 100. The obtained results of interface shapes and flow properties quantitatively agree well with analytical and numerical benchmark solutions. More importantly, the total mass of each phase is accurately conserved in the present solutions. In addition, the mass correction term is in the order of $10^{-5}\sim10^{-4}$ in all cases considered in this work, which is very small. This small value of the mass correction term and the performance of the present approach verify the rationality of the assumption that the distribution of mass loss or increase in the interfacial zone is uniform. It is believed that the present mass-conserved DI approach is a promising tool for simulating multiphase flows with large density ratio.

References

[1] D.M. Anderson, G.B. McFadden, A.A. Wheeler, Diffuse-interface methods in fluid mechanics, Annu. Rev. Fluid Mech. 30 (1998) 139–165.
[2] M.E. Gurtin, D. Polignone, J. Vinals, Two-phase binary fluids and immiscible fluids described by an order parameter, Math. Models Methods Appl. Sci. 6 (1996) 815–831.
[3] F. Boyer, A theoretical and numerical model for the study of incompressible mixture flows, Comput. Fluids 31 (2002) 41–68.
[4] D. Jacqmin, Calculation of two-phase Navier–Stokes flows using phase-field modeling, J. Comput. Phys. 155 (1999) 96–127.
[5] P. Yue, J.J. Feng, C. Liu, J. Shen, A diffuse-interface method for simulating two-phase flows of complex fluids, J. Fluid Mech. 515 (2004) 293–317.
[6] H. Ding, P.D.M. Spelt, C. Shu, Diffuse interface model for incompressible two-phase flows with large density ratios, J. Comput. Phys. 226 (2007) 2078–2095.
[7] A. Gupta, R. Kumar, Lattice Boltzmann simulation to study multiple bubble dynamics, Int. J. Heat Mass Transf. 51 (2008) 5192–5203.
[8] H. Huang, J.-J. Huang, X.-Y. Lu, A mass-conserving axisymmetric multiphase lattice Boltzmann method and its application in simulation of bubble rising, J. Comput. Phys. 269 (2014) 386–402.
[9] X. He, S. Chen, R. Zhang, A lattice Boltzmann scheme for incompressible multiphase flow and its application in simulation of Rayleigh–Taylor instability, J. Comput. Phys. 152 (1999) 642–663.
[10] H. Liu, Y. Zhang, A.J. Valocchi, Modeling and simulation of thermocapillary flows using lattice Boltzmann method, J. Comput. Phys. 231 (2012) 4433–4453.
[11] H. Liu, Y. Zhang, Phase-field modeling droplet dynamics with soluble surfactants, J. Comput. Phys. 229 (2010) 9166–9187.
[12] L.K. Antanovskii, A phase field model of capillarity, Phys. Fluids 7 (1995) 747–753.
[13] D. Jasnow, J. Viñals, Coarse-grained description of thermo-capillary flow, Phys. Fluids 8 (1996) 660–669.
[14] Z.L. Guo, C. Shu, Lattice Boltzmann Method and Its Applications in Engineering, World Scientific Publishing, 2013.
[15] X. Shan, H. Chen, Lattice Boltzmann model for simulating flows with multiple phases and components, Phys. Rev. E 47 (1993) 1815–1819.
[16] M.R. Swift, E. Orlandini, W.R. Osborn, J.M. Yeomans, Lattice Boltzmann simulations of liquid–gas and binary fluid systems, Phys. Rev. E 54 (1996) 5041–5052.
[17] T. Inamuro, T. Ogata, S. Tajima, N. Konishi, A lattice Boltzmann method for incompressible two-phase flows with large density differences, J. Comput. Phys. 198 (2004) 628–644.
[18] T. Lee, C.-L. Lin, A stable discretization of the lattice Boltzmann equation for simulation of incompressible two-phase flows at high density ratio, J. Comput. Phys. 206 (2005) 16–47.
[19] H.W. Zheng, C. Shu, Y.T. Chew, A lattice Boltzmann model for multiphase flows with large density ratio, J. Comput. Phys. 218 (2006) 353–371.
[20] Y. Wang, C. Shu, H.B. Huang, C.J. Teo, Multiphase lattice Boltzmann flux solver for incompressible multiphase flows with large density ratio, J. Comput. Phys. 280 (2015) 404–423.

[21] J.Y. Shao, C. Shu, H.B. Huang, Y.T. Chew, Free-energy-based lattice Boltzmann model for the simulation of multiphase flows with density contrast, Phys. Rev. E 89 (2014) 033309.
[22] T. Lee, L. Liu, Lattice Boltzmann simulations of micron-scale drop impact on dry surfaces, J. Comput. Phys. 229 (2010) 8045–8063.
[23] Y. Sui, H. Ding, P.D.M. Spelt, Numerical simulations of flows with moving contact lines, Annu. Rev. Fluid Mech. 46 (2014) 97–119.
[24] L. Zheng, T. Lee, Z. Guo, D. Rumschitzki, Shrinkage of bubbles and drops in the lattice Boltzmann equation method for nonideal gases, Phys. Rev. E 89 (2014) 033302.
[25] R.G.M. van der Sman, S. van der Graaf, Emulsion droplet deformation and breakup with Lattice Boltzmann model, Comput. Phys. Commun. 178 (2008) 492–504.
[26] H. Huang, H. Zheng, X.Y. Lu, C. Shu, An evaluation of a 3D free-energy-based lattice Boltzmann model for multiphase flows with large density ratio, Int. J. Numer. Methods Fluids 63 (2010) 1193–1207.
[27] S. Aland, A. Voigt, Benchmark computations of diffuse interface models for two-dimensional bubble dynamics, Int. J. Numer. Methods Fluids 69 (2012) 747–761.
[28] H. Ding, C.J. Yuan, On the diffuse interface method using a dual-resolution Cartesian grid, J. Comput. Phys. 273 (2014) 243–254.
[29] G.H. Son, A numerical method for bubble motion with phase change, Numer. Heat Transf., Part B, Fundam. 39 (2001) 509–523.
[30] J. Chao, R. Mei, R. Singh, W. Shyy, A filter-based, mass-conserving lattice Boltzmann method for immiscible multiphase flows, Int. J. Numer. Methods Fluids 66 (2011) 622–647.
[31] Y. Wang, C. Shu, C.J. Teo, Thermal lattice Boltzmann flux solver and its application for simulation of incompressible thermal flows, Comput. Fluids 94 (2014) 98–111.
[32] Y. Wang, C. Shu, C.J. Teo, Development of LBGK and incompressible LBGK-based lattice Boltzmann flux solvers for simulation of incompressible flows, Int. J. Numer. Methods Fluids 75 (2014) 344–364.
[33] X.-D. Liu, S. Osher, T. Chan, Weighted essentially non-oscillatory schemes, J. Comput. Phys. 115 (1994) 200–212.
[34] S. Hysing, S. Turek, D. Kuzmin, N. Parolini, E. Burman, S. Ganesan, L. Tobiska, Quantitative benchmark computations of two-dimensional bubble dynamics, Int. J. Numer. Methods Fluids 60 (2009) 1259–1288.
[35] J. Kim, A continuous surface tension force formulation for diffuse-interface models, J. Comput. Phys. 204 (2005) 784–804.